Cement and Concrete Research (2009) 39:9, 805-813

Assessing the influence of ITZ on the steady-state chloride diffusivity of concrete using a numerical model

Jian-jun Zheng [a]*, Hong S. Wong [b] and Nick R. Buenfeld [b]

[a] Faculty of Civil Engineering and Architecture, Zhejiang University of Technology, Hangzhou 310014, PR China

[b] Concrete Durability Group, Department of Civil and Environmental Engineering, Imperial College London, SW7 2AZ, UK

ABSTRACT

In this study, the influence of the aggregate-cement paste interfacial transition zone (ITZ) on the steady-state chloride diffusivity of mortars and concretes was examined using a semi-empirical, three-phase composite sphere model. Mortars and concretes were modelled as three-phase composites consisting of the aggregate, bulk cement paste and an inhomogeneous ITZ. The latter was divided into a series of homogenous concentric shell elements of equal thickness. The initial porosity and cement gradients at the ITZ were first estimated from the overall water/cement ratio (w_0/c). The evolution of the porosity, solid hydration products and remnants of unreacted cement were then calculated from the hydration degree and local water/cement ratio (w/c) using Powers' empirical model. Based on the Laplacian equation, an element transfer matrix was derived analytically to predict the steady-state chloride diffusivity. The model was calibrated using available experimental data and then applied to perform a sensitivity analysis to evaluate the effects of aggregate content, water/cement ratio, curing period, ITZ width, maximum aggregate size and aggregate gradation on diffusivity. Some of these variables are impractical to quantify by laboratory experimentation. Implications of the findings with regards to the role of ITZ on mass transport properties are discussed.

Keywords: Interfacial transition zone (A); diffusion (B); transport properties (B); microstructure (B); modeling (E); transfer matrix method.

---

*Corresponding author.

E-mail address: jjzheng@zjut.edu.cn (Jian-jun Zheng).

1. Introduction

The durability of most concrete structures is determined by their resistance to penetration of external deleterious species, such as chloride ions. Thus, the ability to estimate the transport properties of a concrete from its mixture proportions and microstructure is attractive, as it would assist the development of service life prediction models and durability-based design codes. However, the microstructure of concrete is complex and its transport properties are influenced by many interacting parameters. This study aims to use a numerical model to explore the relative influences of these parameters and to determine those having the most significant effect on the steady state chloride diffusivity of concrete. Chloride diffusion was selected as the transport process of interest for this study because it is crucial to one of the most widespread and problematic deterioration processes affecting concrete structures, chloride-induced reinforcement corrosion. This particular transport coefficient, i.e. steady state chloride diffusivity as measured in a diffusion cell test, was selected because it is required in mechanistic models of chloride transport that treat chloride ion diffusion and chloride binding separately, but it is extremely time-consuming to measure on representatively thick concrete specimens [1].

At the most basic level, concrete can be viewed as consisting of aggregate particles distributed in a continuous cement paste matrix. Most aggregates used in concrete are dense compared with the paste and so are assumed to allow negligible transport through them. However, the cement paste region surrounding each aggregate particle, i.e. the ITZ, contains higher porosity and lower cement content relative to the bulk cement paste regions farther away and is usually accorded a separate phase. The ITZ occupies a significant fraction of the total paste volume in practical mortars and concretes, and so the property of this phase is expected to have an influence on the overall behaviour of the composite. Indeed, modelling work has found that the ITZ forms an interconnected network even for a modest width of 10-20μm [2], while experimental studies on mortars have observed an increase in the paste porosity due to the presence of the porous ITZs [3].

However, available experimental studies on mortars and concretes, where the aggregate content is systematically increased to change the ITZ volume fraction, do not provide a clear answer as to whether the ITZ has a significant effect on bulk transport properties [4]. For example, some studies have found that the ITZ has a significant influence on the chloride diffusivity [5, 6], while results from other studies seem to suggest otherwise [3, 7, 8]. These conflicting results from different sources underscore the difficulty in isolating the ITZ effect

through experimental studies, where other important parameters that influence transport inevitably vary, when preparing and testing samples with different aggregate contents.

Because a large number of related factors have the potential to influence transport properties, many experiments need to be carried out in order to understand their significance and interactions, and even so, may not be able to isolate all of these effects. In this study, a numerical model is first developed to estimate the chloride diffusivity of conventional concretes. The model is then used to carry out a sensitivity analysis to examine the significance of various parameters, in particular the influence of the ITZ on chloride diffusivity.

2. Modelling techniques

2.1. Overview

The microstructure of concrete is inherently complex and variable, so some approximation is inevitable when attempting to model its effect on bulk properties. In this study, we only consider the case of diffusion under saturated and steady-state conditions. To simplify analysis, the aggregates are modelled as polydispersed spheres and the ITZs as shells of certain width that extend from the aggregate particles. The volume fractions of the ITZ and bulk paste are calculated from the ITZ width, aggregate content and size distribution. To model the microstructure development, the initial distribution of cement particles from the aggregate surface is first specified using an empirical equation with the overall water/cement ratio (w_0/c) and ITZ width as parameters that define the shape of the gradient. A hydration model is then executed and the change in phase composition of the ITZ and bulk paste is followed as hydration proceeds. After a desired hydration degree is achieved, the capillary and gel porosity is calculated as a function of distance from the aggregate surface and converted into diffusivity values using a previously derived relationship. These values are then used as inputs into the three-phase composite sphere model to estimate the diffusivity of the overall system comprised of the aggregate, ITZ and bulk paste.

2.2. Three-phase composite sphere model

A three-phase composite sphere model shown in Fig. 1a is used to represent the concrete matrix, where the inner sphere is the aggregate phase with radius r_a, surrounded by a concentric ITZ shell of width $r_b - r_a$. The ITZ is further subdivided into N concentric shell elements of equal thickness, where each shell element is composed of unreacted cement, hydration products and pores. The aggregate and the ITZ shells are embedded in bulk paste matrix of thickness $r_c - r_b$. The shell elements are assumed to be homogeneous and isotropic in composition and transport property. The values of r_a, r_b and r_c are defined such that the volume fractions of the aggregates, ITZ and bulk paste in the model match those values calculated for the actual sample (shown next). This approach of homogenisation at the mesoscale is broadly similar to previous models such as the n-layered spherical inclusion model that has been applied to study elasticity, thermoelasticity, electrical/thermal conductivity and ionic diffusivity of composite materials [9-11]. However, unlike some effective medium based models, the ITZ is not assumed here to be a single shell of uniform property, but the composition and diffusivity of each ITZ shell is allowed to vary with distance from the aggregate surface and with the progress of hydration as shown in Fig. 1b.

To determine the volume fractions of the ITZ and bulk paste, the aggregate size distribution is required and this can either be generated from typical sieve analysis, or assumed to follow a particular gradation such as Fuller or Equal Volume Fraction (EVF) that represent the lower and upper bounds of typical aggregate gradation respectively [12]. This can be expressed as

$$p(D) = \frac{nD_{min}^n D_{max}^n}{(D_{max}^n - D_{min}^n)D^{n+1}} \quad (1)$$

where $p(D)$ is the probability density function for the aggregate distribution in terms of the number of aggregate particles, D is the diameter of aggregate particles, which varies between the minimum aggregate diameter D_{min} and the maximum aggregate diameter D_{max}, and n is a coefficient denoting the type of aggregate gradation (2.5 for Fuller gradation and 3 for EVF gradation).

The volume fraction of ITZ is then computed, taking into account the overlapping of ITZ shells in samples containing large aggregate contents. This is carried out analytically using the 'void exclusion probability' derived by Lu & Torquato [13] for the polydispersed spheres system, and as described in Bentz & Garboczi [10]. When applied to our case, the void exclusion probability is basically the volume fraction of the space not

118 occupied by all the spheres and ITZ shells, i.e. fraction of the bulk paste. Accordingly, the ITZ volume fraction
119 f_i for an ITZ width of h can be expressed as

120 $$f_i = (1 - f_a)[1 - \exp(-\pi\rho(t_1 h + t_2 h^2 + t_3 h^3))] \quad (2)$$

121 where f_a is the aggregate volume fraction, ρ is the total number of aggregate particles per unit volume, and t_1,
122 t_2 and t_3 are coefficients defined in terms of the mean aggregate radius $\langle R \rangle$ and the mean square aggregate
123 radius $\langle R^2 \rangle$, over the entire aggregate size distribution.

124 $$t_1 = \frac{4\langle R^2 \rangle}{1 - f_a} \quad (3a)$$

125 $$t_2 = \frac{4\langle R \rangle}{1 - f_a} + \frac{8\pi\rho\langle R^2 \rangle^2}{(1 - f_a)^2} \quad (3b)$$

126 $$t_3 = \frac{4}{3(1 - f_a)} + \frac{16\pi\rho\langle R \rangle\langle R^2 \rangle}{3(1 - f_a)^2} + \frac{64\lambda\pi^2\rho^2\langle R^2 \rangle^3}{27(1 - f_a)^3} \quad (3c)$$

127 The parameter λ in Eq. (3c) is equal to 0, 2, or 3, depending on the approximation used in the derivation by Lu
128 & Torquato [13]. However, Garboczi & Bentz [10] observed that the value for λ does not make much
129 difference to the calculated ITZ volume fraction, and the best agreement with numerical simulation results was
130 obtained when $\lambda = 0$. Thus λ is taken as zero in this paper. Once the ITZ volume fraction is known, the
131 volume fraction of bulk paste f_m is obtained by simple subtraction.
132
133 2.3. Microstructure and hydration model
134
135 To model the microstructure development of the cement paste, we begin by specifying the initial distribution of
136 cement particles at the time of mixing. This was previously estimated by Crumbie [14] who measured the
137 distributions of unreacted cement, porosity and hydration products after various hydration times using
138 backscattered electron microscopy. From these, the initial distribution of the cement particles can be back-
139 calculated and the results for concretes with different w_0/c ratios are reproduced in Fig. 2. Crumbie [14] found
140 that the ITZ width is between 20-30μm and that the porosity tends towards 100% at the interface. As expected,
141 the width of the ITZ appears to be related to the cement particle size, but is independent of the aggregate size and
142 w_0/c ratio, although the latter influences the gradient of the cement distribution.
143

Using the data from Crumbie [14], we can approximate the initial distribution of cement particles $f_c(r)$ with the following equation:

$$f_c(r) = \begin{cases} f_{c,bulk} \sum_{j=1}^{4} (b_j / b_0)[(r - r_a)/(r_b - r_a)]^j, & r_a \le r < r_b \\ f_{c,bulk}, & r_b \le r \le r_c \end{cases} \quad (4)$$

where $f_{c,bulk}$ is the cement volume fraction in the bulk paste, r is the distance from the centre of the aggregate, r_a, r_b and r_c are as defined in Fig. 1b, b_0 is the sum of b_j (i.e. $b_0 = \sum b_j$) and b_j is a series of empirical functions expressed in terms of w_0/c ratio, obtained from least squares analysis:

$$\begin{aligned} b_1 &= 4.670 - 5.228(w_0/c) \\ b_2 &= -10.569 + 12.700(w_0/c) \\ b_3 &= 9.950 - 12.195(w_0/c) \\ b_4 &= -3.397 + 4.195(w_0/c) \end{aligned} \quad (5)$$

The volume fraction of cement in the bulk paste $f_{c,bulk}$ can be calculated from w_0/c ratio, cement density ρ_c and the volume fractions of the bulk paste and ITZ as follows. Consider that the total volume of cement in the composite sphere V_c is the sum of the volume of cement located in the ITZ, $V_{c,ITZ}$, and in the bulk cement paste, $V_{c,bulk}$, i.e.

$$V_c = V_{c,ITZ} + V_{c,bulk} = \frac{4\pi(r_c^{\,3} - r_a^{\,3})}{3[1 + \rho_c(w_0/c)]} \quad (6)$$

$V_{c,ITZ}$ can be obtained by integrating Eq. (4) from $r = r_a$ to r_b:

$$V_{c,ITZ} = \int_{r_a}^{r_b} 4\pi r^2 f_c(r)\,dr = 8\pi f_{c,bulk} \sum_{j=1}^{4} \sum_{k=1}^{3} \frac{b_j r_a^{\,(3-k)} (r_b - r_a)^k}{b_0 (j+k)[(k-1)!][(3-k)!]} \quad (7)$$

and $V_{c,bulk}$ is the product of $f_{c,bulk}$ and the volume of the bulk paste:

$$V_{c,bulk} = \frac{4\pi(r_c^{\,3} - r_b^{\,3}) f_{c,bulk}}{3} \quad (8)$$

Substituting Eqs. (7) and (8) into Eq. (6) and solving for $f_{c,bulk}$ yields:

$$f_{c,bulk} = \frac{(r_c^{\,3} - r_a^{\,3})}{[1 + \rho_c(w_0/c)]\left[(r_c^{\,3} - r_b^{\,3}) + 6\pi \sum_{j=1}^{4} \sum_{k=1}^{3} \frac{b_j r_a^{\,(3-k)} (r_b - r_a)^k}{b_0 (j+k)[(k-1)!][(3-k)!]}\right]} \quad (9)$$

Fig. 2 shows that the agreement between Eq. (4) and the data from Crumbie [14]. The correlation coefficients for the regression analysis are 0.9982 and 0.9978 for w_0/c ratio of 0.4 and 0.6 respectively. Note that this approach does not simulate the packing of individual cement grains on the aggregate surface. The cement particles are merely distributed to recreate the gradients measured by Crumbie [14] as a function of w_0/c ratio, but allowing us to treat the ITZ width as a freely variable parameter. With the initial cement distribution described, the local water/cement ratio (w/c) at any point in the ITZ and bulk paste can be determined as follows:

$$w/c = \frac{1 - f_c(r)}{\rho_c f_c(r)} \tag{10}$$

After the initial distribution of the cement particles, simple empirical equations are used to model the hydration reactions between cement and water. The cement particles are allowed to hydrate and the change in phase composition of the ITZ shells and bulk paste is followed with the progress of hydration. The hydration of cement is assumed to occur via a dissolution and precipitation process, and the reaction rates are as described in the model by Parrot & Killoh [15]. In this approach, the rate of hydration of a particular clinker phase $R_{i,t}$ is expressed by a set of three equations below, where the lowest value of $R_{i,t}$ at any time is taken as the rate controlling step and used to calculate the instantaneous degree of hydration:

Nucleation and growth: $$R_{i,t} = \frac{K_1}{N_1}(1-\alpha_{i,t})[-\ln(1-\alpha_{i,t})]^{1-N_1} \tag{11a}$$

Diffusion: $$R_{i,t} = \frac{K_2(1-\alpha_{i,t})^{2/3}}{1-(1-\alpha_{i,t})^{1/3}} \tag{11b}$$

Formation of hydration shell: $$R_{i,t} = K_3(1-\alpha_{i,t})^{N_3} \tag{11c}$$

where $\alpha_{i,t}$ is the degree of hydration of clinker phase i (C_3S, C_2S, C_3A and C_4AF) at time t (in days) and K_1, N_1, K_2, K_3, and N_3 are empirical constants from Parrot & Killoh [15], as listed in Table 1. The degree of hydration at time $t + \Delta t$ is then expressed as:

$$\alpha_{i,t+\Delta t} = \alpha_{i,t} + \Delta t R_{i,t} \tag{12}$$

where Δt is the time interval for integration. The overall degree of hydration α is calculated as a weighted average of the degrees of hydration of the clinker phases. For this study, hydration is assumed to occur at room temperature so the effect of temperature on the rate constants is not considered, although this is possible in

Parrot & Killoh's model. However the effect of water/cement ratio is accounted for by reducing the degree of hydration by a factor β as follows:

$$\beta = \begin{cases} [1 + 4.444(w/c) - 3.333\alpha]^4 \text{ for } \alpha > 1.333(w/c) \\ 1, \quad \text{for } \alpha \le 1.333(w/c) \end{cases} \tag{13}$$

As the cement hydrates, the originally water-filled spaces (capillary pores) become progressively filled with hydration products due to increase in total solids volume. However, the main hydration product (C-S-H) also contains pores, i.e gel pores, and these will increase in volume as hydration continues. According to Powers & Brownyard's [16] model (as summarised by Hansen [17]), the volume fractions of capillary f_{cap} and gel pores f_{gel} are related to the water/cement ratio and the degree of hydration, hence the total porosity f_p is:

$$f_p = f_{cap} + f_{gel} = \frac{(w/c) - 0.36\alpha}{(w/c) + 0.32} + \frac{0.19\alpha}{(w/c) + 0.32} \tag{14}$$

Note that the above equation was derived using specific values of chemical and physical bound water, and chemical shrinkage for the hydration of typical Portland cements under room temperature conditions [17]. Thus, the equation is likely to be less accurate for other systems such as those containing supplementary cementitious materials. Assuming that the hydration products are deposited close to the cement from which they are formed, this equation can then be used to calculate the porosity of the ITZ shells and bulk paste at any location and time, from the local water/cement ratio (Eq. 10) and degree of hydration (Eq. 12). Fig. 3 shows an example of the simulated distributions of unreacted cement, capillary and gel pores, and hydration products for a concrete at 0.4 w_0/c ratio that has hydrated for 28 days.

2.4. Calculation of chloride diffusivity

Initially, the ITZ contains a higher water/cement ratio and more porosity than the bulk paste. As the cement hydrates, the porosity is reduced throughout, but remains higher in the ITZ. The previous section described how the porosity can be quantified as a function of distance from the aggregate surface at any time during hydration. The next step is to apply these results to define the diffusivities of the ITZ shells and bulk paste in our composite model (Fig. 1b).

Zheng & Zhou [18] presented a semi-empirical equation for the steady-state chloride diffusivity of Portland cement pastes, which was derived by considering the cement paste as consisting of impermeable solids and pore space. By introducing a hypothetical homogeneous medium of non-zero diffusivity and applying the effective medium model described in Koelman & de Kuijper [19], the chloride diffusivity of the cement paste was shown to be a function of the porosity and the diffusivity of chloride ions in the pore solution:

$$D_{cp} = \frac{2 f_p^{2.75} D_p}{f_p^{1.75}(3 - f_p) + 14.4(1 - f_p)^{2.75}} \tag{15}$$

where D_{cp} and D_p are the chloride diffusivity of the cement paste and the pore solution respectively. The exponents for porosity are derived from percolation theory [19, 20] and the value 14.4 is a fitting parameter from two sets of experimental data for ASTM Type 1 cement pastes with w_0/c ratios ranging from 0.4 to 0.8 [18]. We note that D_p is the only non-measurable parameter in the model and needs to be calibrated with experimental results from neat cement pastes. D_p accounts for pore geometry effects and physico-chemical interactions, and so should be significantly lower than the diffusivity of chloride ions in bulk water (=2.0×10^{-9} m^2/s at 20˚C) [21]. Eq. (15) has been further tested on three independent sets of experimental data showing reasonably good agreement [18]. It also appears to fit both experimental data obtained by using simple diffusion cells or electro-migration.

Once the ITZ shells and bulk paste have been assigned with their respective diffusivities, the final step in the model is to derive the effective diffusivity of the composite sphere model by applying a concentration gradient in the radial direction and using a transfer matrix method [9]. For steady-state diffusion, the chloride content $C(r,\varphi,\theta)$ in a homogeneous and isotropic medium should satisfy the following governing equation [22]:

$$\nabla^2 C(r,\varphi,\theta) = 0 \tag{16}$$

where ∇^2 is the Laplacian operator in spherical polar coordinates with the origin at the common centre of the spheres; r, φ and θ are the distance from the centre, and the polar and azimuthal angles respectively.

$$\nabla^2 = \frac{1}{r^2}\frac{\partial}{\partial r}\left(r^2 \frac{\partial}{\partial r}\right) + \frac{1}{r^2 \sin\theta}\frac{\partial}{\partial \theta}\left(\sin\theta \frac{\partial}{\partial \theta}\right) + \frac{1}{r^2 \sin^2\theta}\frac{\partial^2}{\partial \varphi^2} \tag{17}$$

The aggregate phase is assumed to have zero diffusivity so the radial flux $q(r,\varphi,\theta)$ at the aggregate surface ($r = r_a$) and at the outer boundary of the composite sphere ($r = r_c$) can be written as:

242 $q(r_a,\varphi,\theta)=0$ and $q(r_c,\varphi,\theta)=\overline{q}_{N+1}\cos\theta$ (18)

243 From the governing Eq. 16 and the boundary conditions in Eq. 18, it can be shown that the general solution for
244 the chloride content and corresponding radial flux in the *i*-th homogeneous spherical shell element are in the
245 form of [22]:

246 $$C(r,\varphi,\varphi)=\left(A_{1i}r+\frac{A_{2i}}{r^2}\right)\cos\theta \text{ and } q(r,\varphi,\varphi)=-\overline{D}_i\left(A_{1i}-\frac{2A_{2i}}{r^3}\right)\cos\theta \quad (19)$$

247 where A_{1i} and A_{2i} are constants that can be determined from the boundary conditions. If the chloride content
248 and radial chloride flux at $r=r_i$ are expressed as $\overline{C}_i\cos\theta$ and $\overline{q}_i\cos\theta$ respectively, substitution of $r=r_i$ and
249 $r=r_{i+1}$ into Eq. 19 yields:

250 $$\overline{C}_i=\left(A_{1i}r_i+\frac{A_{2i}}{r_i^{\,2}}\right) \text{ and } \overline{q}_i=-\overline{D}_i\left(A_{1i}-\frac{2A_{2i}}{r_i^{\,3}}\right) \quad (20a)$$

251 $$\overline{C}_{i+1}=\left(A_{1i}r_{i+1}+\frac{A_{2i}}{r_{i+1}^{\,2}}\right) \text{ and } \overline{q}_{i+1}=-\overline{D}_i\left(A_{1i}-\frac{2A_{2i}}{r_{i+1}^{\,3}}\right) \quad (20b)$$

252 By rearranging Eq. 20 and eliminating A_{1i} and A_{2i}, $\overline{C}_{i+1}$ and $\overline{q}_{i+1}$ can be expressed in terms of $\overline{C}_i$ and $\overline{q}_i$ as:

253 $$\begin{Bmatrix}\overline{C}_{i+1}\\ \overline{q}_{i+1}\end{Bmatrix}=[t^i]\begin{Bmatrix}\overline{C}_i\\ \overline{q}_i\end{Bmatrix} \quad (21)$$

254 where $[t_i]$ is a 2×2 element transfer matrix and its four elements are as follows:

255 $$t_{11}^{\ i}=\frac{r_i^{\,3}+2r_{i+1}^{\,3}}{3r_ir_{i+1}^{\,2}},\ t_{12}^{\ i}=\frac{r_i^{\,3}-r_{i+1}^{\,3}}{3\overline{D}_ir_{i+1}^{\,2}},\ t_{21}^{\ i}=\frac{2\overline{D}_i(r_i^{\,3}-r_{i+1}^{\,3})}{3r_ir_{i+1}^{\,3}},\ t_{22}^{\ i}=\frac{2r_i^{\,3}+r_{i+1}^{\,3}}{3r_{i+1}^{\,3}} \quad (22)$$

256 By iterating Eq. 22, one can then derive an equation that relates $\overline{C}_{N+1}$ and $\overline{q}_{N+1}$ to $\overline{C}_1$ and $\overline{q}_1$ according to the
257 principle of transfer matrix method [23]:

258 $$\begin{Bmatrix}\overline{C}_{N+1}\\ \overline{q}_{N+1}\end{Bmatrix}=[T]\begin{Bmatrix}\overline{C}_1\\ \overline{q}_1\end{Bmatrix} \quad (23)$$

259 where the global transfer matrix $[T]$ is:

260 $$[T]=\prod_{i=1}^{N+1}[t^{(N+2-i)}] \quad (24)$$

261 It follows from the boundary condition (Eq. 18) that $\overline{q}_1=0$ and thus:

262 $$\overline{q}_{N+1}=\frac{T_{21}\overline{C}_{N+1}}{T_{11}} \quad (25)$$

If the composite sphere model is considered as a monolithic homogeneous medium with an effective diffusivity D_{con}, it is easily shown that:

$$\overline{q}_{N+1} = -\frac{D_{con}\overline{C}_{N+1}}{r_c} \tag{26}$$

Finally, by comparing Eq. (25) with Eq. (26), it follows that:

$$D_{con} = -\frac{T_{21}r_c}{T_{11}} \tag{27}$$

To apply Eq. (27), it is first necessary to evaluate the effect of the number of ITZ shells, N on the simulation. Obviously, dividing the ITZ into more elements will improve accuracy of the simulation, but at the cost of longer computation time. Fig. 4 shows the effect of N on the calculated diffusivity ratio D_{con}/D_p for concretes with total aggregate volume fraction ranging from 0.2 to 0.8. The simulated concrete has a $w_0/c = 0.5$, aggregate size = 0.15-16mm (Fuller gradation), h = 35μm and curing period of 28 days. It can be seen from Fig. 4 that in all cases, D_{con}/D_p increases with N up to about N =5. For N >5, D_{con}/D_p achieves a relatively stable value, which suggests that the minimum number of ITZ elements required is about six. As a conservative estimate, we will use N =10 for all subsequent simulations.

3. Results

3.1. Comparison with previous experimental results

In this section, we compare the simulated diffusivities from the proposed model with two sets of experimental results found in the literature. The first set, from Delagrave et al. [3], consists of three series of mortars. Series 1 was made of French OPC (CPA-CEM I 42.5) at 0.38 w_0/c ratio and 0.3-3mm natural siliceous sand at 0%, 19% and 57% volume fractions. 10mm thick samples were cured in saturated lime solution for 28 days and then vacuum saturated in a simulated pore solution (0.08M KOH, 0.025M NaOH). The samples were then tested using a two-compartment diffusion cell similar to the one described by Chatterji & Kawamura [24], containing 0.35M NaCl in the simulated pore solution in the upstream compartment. Chloride concentration in the downstream compartment was periodically measured for 15 months and the effective diffusion coefficient was

obtained from the steady-state regime according to Fick's first law. Mortars from Series 2 were made of ASTM Type I cement at 0.45 w_0/c ratio, while mortars from Series 3 were made of ASTM Type III cement at 0.25 w_0/c ratio. Both contained 0.15-0.6mm crushed siliceous sand at 0%, 30% and 50% volume fractions. 15mm thick samples from both series were cured in saturated lime solution for 3 months then vacuum-saturated in deionised water and tested using a migration cell technique similar to the one described by Buenfeld & El-Belbol [25]. The upstream compartment of the migration cell was filled with a 0.5M NaCl in 0.3M NaOH solution, and a 10V potential was applied across the cell. The chloride concentration in the downstream compartment was monitored for 3 weeks and the migration coefficient was obtained from the steady-state regime according to the Nernst-Plank equation.

The second set of data is from Yang & Su [26], who tested mortars made of ASTM Type I cement at a w_0/c ratio of 0.40. The mortars contained 0.15-4.75mm sand at 0%, 10%, 20%, 30% and 40% volume fractions. After demoulding, the 50mm thick samples were cured in water for 12 months and then vacuum saturated in deionised water. The samples were tested using a migration cell similar to the one described earlier, except that a higher 60V potential was used.

To apply the proposed model, the ITZ width, h and the chloride diffusivity in the pore solution, D_p need to be predetermined. The ITZ width is known to be related to the cement particle size, and typical values of 20 to 50μm have been reported in the literature. Thus, the lower and upper bounds for the simulation can be made by taking h equal to 20 and 50μm respectively. In well-hydrated and very dense systems, the ITZ may be very small or even non-existent, so we will simulate the case of a thin ITZ (5μm) for comparison. The chloride diffusivity in the pore solution D_p, however, is dependent on many factors such as the materials and mix proportions, hydration degree, test conditions and pore structure. Unfortunately, there is a lack of data to quantify this relationship, so D_p can only be determined by fitting results of neat pastes. This produces the following D_p values: 2.8×10^{-11}m^2/s, 9.5×10^{-11}m^2/s and 1.9×10^{-11}m^2/s for Series 1, 2 and 3 respectively [3] and 6.2×10^{-11}m^2/s for the samples from Yang & Su [26]. As expected, D_p is significantly lower than the diffusivity in bulk water or in simulated pore solutions (~10^{-10}m^2/s) [27].

Fig. 5 compares the numerical simulations with experimental results, which are plotted against aggregate volume fraction. Note that the actual aggregate size distribution and cement composition from the original references were used as inputs to the proposed model. The measured diffusivities range slightly over one order of magnitude, between 1×10^{-13} and 4.5×10^{-12}m^2/s. The results show that in all cases, the diffusivity decreases with increase in aggregate volume fraction. For samples with w_0/c ratio of 0.38, 0.40 and 0.45 (Figs. 5a, b & d), the measured diffusivities seem to agree well with the estimated values when the ITZ width is taken to be equal to 20μm. The errors are between -5% and +3%, except in one instance (w_0/c =0.38, f_a =0.55) where the diffusivity is under-estimated by 26%. For samples with w_0/c ratio of 0.25 (Fig. 5d), the agreement between the measured diffusivity values and the estimated values appear to be reasonable when a smaller ITZ width of 5μm is assumed. However, the discrepancy here is higher than the previous case, that is -12% and +18% for f_a =0.3 and 0.5 respectively. Nevertheless, the smaller ITZ width is consistent with the expectation for this mix, which has the lowest w_0/c ratio.

3.2. Sensitivity analysis

A sensitivity analysis was carried out using the proposed model to examine the relative influence of w_0/c ratio, curing period, ITZ width and aggregate volume fraction, size and gradation. We plotted the ratio D_{con}/D_p against aggregate volume fraction for four test cases as described in Table 2, which were designed to examine the effect of changing a particular variable on the simulated diffusivity ratio. Results are shown on separate plots for each test case in Fig. 6, plotted on the same scale to facilitate comparison. The percentage change in D_{con}/D_p due to varying each parameter at the simulated range is also given in Table 3.

For all cases, the diffusivity decreases significantly with the increase in aggregate content and samples with large w_0/c ratio and short curing age show the highest change in D_{con}/D_p ratio. For instance, increasing the aggregate content from 0 to 60% decreases the D_{con}/D_p ratio by a factor of three for 0.6 w_0/c, and by a factor of two for 0.4 w_0/c ratio. Fig. 6a shows that a reduction in w_0/c ratio will also cause a significant reduction in D_{con}/D_p, as expected. However, this effect decreases at high aggregate contents. At 0% aggregate, D_{con}/D_p for

0.6 w_0/c ratio is about three times that for 0.4 w_0/c ratio, while at 60% aggregate, D_{con}/D_p for 0.6 w_0/c ratio is about twice that for 0.4 w_0/c ratio.

For samples with equal w_0/c ratio and aggregate content, D_{con}/D_p decreases with the increase in curing age (Fig. 6b) and this effect is again more pronounced at low aggregate contents. When the sample is cured longer, the effect of further hydration on D_{con}/D_p becomes smaller. This is probably due to the fact that the rate of hydration and pore filling is higher at early ages and that the difference in porosity between the ITZ and the bulk cement paste becomes smaller as hydration proceeds.

At equal w_0/c ratio and curing age, increasing the ITZ width results in a small increase in D_{con}/D_p (Fig. 6c). Using a smaller aggregate size and finer gradation (the EVF compared with the Fuller) also increases D_{con}/D_p slightly (Fig. 6d). Nevertheless, comparing Figs. 6 (c & d) with Figs. 6 (a & b), it is evident that the effect of ITZ width and aggregate size on the diffusivity is small compared with aggregate content, w_0/c ratio and curing age.

4. Discussion

The proposed model has several limitations due to the approximations used in its development. Although its agreement with some experimental data appears to be good, it is only strictly valid within the assumptions used and is not expected to be generally applicable. The model contains several empirical relationships and requires calibration with experimental data, which also limits its ability to predict the properties of in-situ concrete. Nevertheless, as stated in the Introduction, our main objective here is to use the model to investigate how different parameters affect the diffusivity, which would otherwise be difficult to ascertain from experiments.

Obviously, real mortars and concretes are far more complicated than the three-phase model presented here. Real aggregate particles are not spheres, and therefore have a larger specific surface and create more ITZ than spherical aggregate particles at the same volume fraction. However, this approximation is not likely to have a huge influence on the estimated diffusivities, as evident from our simulations (Figs. 6c & d).

Some studies have shown that the ITZ width is related to the median size of cement particles used. Our model does not simulate the packing of individual cement particles, but it treats the ITZ width as a variable so that we are not restricted here. In addition, the modelled ITZ is not a single shell of uniform property, but has gradients extending out to its width, which depends on the initial mixture proportions and evolves with hydration. However, the real ITZ microstructure is spatially variable, its width and microstructural gradients are not exhibited uniformly around each and every aggregate particle. Although its average property taken over many locations shows well-defined gradients, its local property is highly variable. The mobility of calcium ions in solution results in preferential nucleation and growth of calcium hydroxide on the aggregate surface, so that the porosity of the ITZ in many locations may be very low due to the presence of these deposits [28]. In our model, this effect is not captured because our approach assumes that the hydration products are always deposited close to the cement from which they form. Bleeding effects may also increase the porosity in other locations. Arguably, mapping an averaged property onto every aggregate particle may be a conservative approach, and this merits further investigation.

Mortars and concretes also contain entrapped or entrained air voids, which are often assumed to play a negligible role in mass transport since they appear isolated, and so can simply be treated as inclusions that dilute the paste matrix. Large air voids would also have their associated ITZs, and in certain cases, may be packed very close to aggregate particles. These void-paste ITZs are potentially more porous than the aggregate-paste ITZs, since aggregates can absorb some excess water in the fresh state and release it later for hydration of the surrounding paste. Modelling work by Bentz et al. [29] found that increasing the amount of empty air voids from 0 to 10% caused a small decrease in chloride diffusivity of concrete, suggesting that the dilution effect is more dominant. However, unlike aggregate particles, air voids may not be treated as inclusions with zero conductivity depending on their degree of saturation. Samples exposed to water for long periods may have air voids that are saturated with water. We do not know if these effects are significant or may cancel out, as there has been no systematic experimental study to establish the effect of saturated air voids on diffusivity.

Structures in service are often cracked due to loading and drying shrinkage, but modelling microcracks and its effect on transport properties is extremely challenging. For samples with high aggregate contents, these localised microcracks could become interconnected, thereby potentially compounding any effect of the ITZ. However, there are some experimental and theoretical studies that show that microcracking has very little effect on

diffusion compared with pressure-induced flow [4, 30, 31]. This is because permeability is influenced by pore size, while diffusivity is more dependent on the total porosity, which is not significantly increased by the microcracks.

In modelling the transport process, we assumed that all pores are saturated and that the only transport mechanism occurring is diffusion in the steady-state regime, where free and bound chlorides are already in equilibrium. Furthermore, we assumed that chloride diffusion occurs in both capillary and gel pores. This is an approximation because it is reasonable to expect that the larger capillary pores would play a dominating role at early ages. When these become filled with hydration products at later ages, diffusion would then occur via the smaller gel pores.

Previous modelling and experimental studies, for example Winslow et al., 1994, have shown that ITZ percolates in samples with high aggregate contents. Our model does not explicitly address this, although it takes the ITZ into account. However, whether or not ITZ percolation influences the composite property depends on the contrast between the ITZ property and that of the bulk matrix [32, 33]. Fig. 7 shows the calculated diffusivity ratio between the ITZ and bulk paste, D_{ITZ}/D_{bulk}, for a range of aggregate contents and ITZ widths, for a concrete with w_0/c ratio of 0.6. The ITZ diffusivity is taken as the average diffusivity of all the ITZ shell elements. It can be observed that the D_{ITZ}/D_{bulk} ratio increases with aggregate content and ITZ width, but is no more than five in the most extreme case. This contrast is considered low, and is not expected to have a significant effect on the overall property.

The sensitivity analysis shows that the aggregate volume fraction, w_0/c ratio, and curing age are the most significant parameters, while the ITZ width, aggregate size and aggregate gradation have less influence on diffusivity. This finding agrees well with the study by Bentz et al. [29]. It suggests that the changes in total paste volume and total porosity due to mix design and curing have a more significant effect on diffusivity. Increasing aggregate content produces more ITZ, but this is accompanied by a decrease in total porosity because more paste is replaced by the non-porous aggregate particles. At constant aggregate content, increasing the ITZ width or using a finer aggregate size creates more porous ITZ, but this is balanced by a denser bulk paste (lower w/c ratio) as a result of water conservation in the mix. These effects tend to cancel each other so that the overall

influence of the ITZ width and aggregate size is negligible within the range examined. Therefore, the influence of ITZ on the overall diffusivity is not significant, despite it being on average more porous and itself having a diffusivity that is several times that of the bulk paste.

5. Conclusions

In this study, a numerical method for estimating the steady-state chloride diffusivity of mortars and concretes was presented. Mortars and concretes were approximated as three-phase composites representing the non-porous aggregate, bulk cement paste and an inhomogeneous ITZ. The model was calibrated using experimental data and then applied to examine the influence of several parameters on diffusivity. It was found that the chloride diffusivity decreases with increase in aggregate volume fraction, curing period and maximum aggregate diameter, but increases with increase in w_0/c ratio and ITZ width. The most significant parameters however, were the aggregate content, w_0/c ratio and curing age, which control the total porosity of the composite. The net effect of the ITZ on the overall diffusivity was actually small, although its porosity and local diffusivity are higher than those of the bulk paste. This indicates that diffusivity is governed by the volume fraction and microgeometry of the entire pore structure within the cement paste, and not just that within the porous ITZ.

Acknowledgements

The financial support from the National Natural Science Foundation (Grant No. 50578147 and 50878196) and the Natural Science Foundation of Zhejiang Province (Grant No. Y107638), of the People's Republic of China and the UK Engineering & Physical Sciences Research Council (F002955) is gratefully acknowledged.

References

[1] G.K. Glass, N.R. Buenfeld, Theoretical assessment of the steady state diffusion cell test, J. Mater. Sci. 33 (21) (1998) 5111-5118.

[2] D.N. Winslow, M.N. Cohen, D.P. Bentz, K.A. Snyder, E.J. Garboczi, Percolation and pore structure in mortars and concrete, Cem. Concr. Res. 24 (1) (1994) 25-37.

[3] A. Delagrave, J.P. Bigas, J.P. Ollivier, J. Marchand, M. Pigeon, Influence of the interfacial zone on the chloride diffusivity of mortars, Adv. Cem. Based Mater. 5 (3-4) (1997) 86-92.

[4] H.S. Wong, M. Zobel, N.R. Buenfeld, R.W. Zimmerman, Influence of the interfacial transition zone and microcracking on the diffusivity, permeability and sorptivity of cement-based materials after drying, Mag. Concrete Res. (2008) (submitted).

[5] P. Halamickova, R.J. Detwiler, D.P. Bentz, E.J. Garboczi, Water permeability and chloride ion diffusion in Portland cement mortars: Relationship to sand content and critical pore diameter, Cem. Concr. Res. 25 (4) (1995) 790-802.

[6] A.H. Ashbridge, G.A. Chadbourn, C.L. Page, Effects of metakaolin and the interfacial transition zone on the diffusion of chloride ions through cement mortars, Cem. Concr. Res. 31 (11) (2001) 1567-1572.

[7] H. Hornain, J. Marchand, V. Duhot, M. Moranville-Regourd, Diffusion of chloride ions in limestone filler blended cement pastes and mortars, Cem. Concr. Res. 25 (8) (1995) 1667-1678.

[8] N.R. Buenfeld, E. Okundi, Effect of cement content on transport in concrete, Mag. Concrete Res. 50 (4) (1998) 339-351.

[9] E. Hervé, A. Zaoui, n-Layered inclusion-based micromechanical modelling, Int. J. Eng. Sci. 31 (1) (1993) 1-10.

[10] E.J. Garboczi, D.P. Bentz, Analytical formulas for interfacial transition zone properties, Adv. Cem. Based Mater. 6 (3-4) (1997) 99-108.

[11] S. Caré, E. Hervé, Application of a n-phase model to the diffusion coefficient of chloride in mortar, Transport Porous Med. 56 (2) (2004) 119-135.

[12] J.J. Zheng, C.Q. Li, Three-dimensional aggregate density in concrete with wall effect, ACI Mater. J. 99 (6) (2002) 568-575.

[13] B.L. Lu, S. Torquato, Nearest-surface distribution functions for polydispersed particle system, Phys. Rev. A 45 (8) (1992) 5530-5544.

[14] A.K. Crumbie, Characterisation of the microstructure of concrete, PhD Thesis, Imperial College London, 1994.

[15] L.J. Parrot, D.C. Killoh, Prediction of cement hydration, Br. Ceram. Proc. 35 (1984) 41-53.

[16] T.C. Powers, T.L. Brownyard, Studies of the physical properties of hardened Portland cement paste, Bull. 22, Res. Lab. of Portland Cement Association, Skokie, IL, USA, reprinted from J. Am. Concr. Inst. (Proc.) 43 (1947) 101-132, 249-336, 469-504, 549-602, 669-712, 845-880, 933-992.

491 [17] T.C. Hansen, Physical structure of hardened cement paste: A classical approach, Mater. Struct. 19 (6)
492 (1986) 423-436.
493 [18] J.J. Zheng, X.Z. Zhou, Analytical solution for the chloride diffusivity of hardened cement paste, J.
494 Mater. Civil Eng. 20 (5) (2008) 384-391.
495 [19] J.M.V.A. Koelman, A. de Kuijper, An effective medium model for the electric conductivity of an N-
496 component anisotropic and percolating mixture, Physica A, 247 (1) (1997) 10-22.
497 [20] P.Z. Wong, J. Koplik, J.P. Tomanic, Conductivity and permeability of rocks, Phys. Rev. B 30 (11)
498 (1984) 6606-6614.
499 [21] R. Mills, V.M.M. Lobo, Self-Diffusion in Electrolyte Solutions: A Critical Examination of Data
500 Compiled from the Literature, Elsevier, Amsterdam, 1989.
501 [22] J. Crank, The Mathematics of Diffusion, Clarendon Press, Oxford, 1975.
502 [23] T. Alexander, Transfer Matrix Method, Kluwer Academic publishers, Boston, 1988.
503 [24] S. Chatterji, M. Kawamura, A critical reappraisal of ion diffusion through cement based materials: Part
504 1: Sample preparation, measurement technique and interpretation of results, Cem. Concr. Res. 22 (4)
505 (1992) 525-530.
506 [25] N.R. Buenfeld, S. El-Belbol, Rapid estimation of chloride diffusion coefficient in concrete-comment,
507 Mag. Concrete Res. 43 (1) (1991) 135-139.
508 [26] C.C. Yang, J.K. Su, Approximate migration coefficient of interfacial transition zone and the effect of
509 the aggregate content on the migration coefficient of mortar, Cem. Concr. Res. 32 (10) (2002) 1559-
510 1565.
511 [27] P. Pivonka, C. Hellmich, D. Smith, Microscopic effects on chloride diffusivity of cement pastes - a
512 scale-transition analysis, Cem. Concr. Res. 34 (12) (2004) 2251-2260.
513 [28] H.S. Wong, N.R. Buenfeld, Euclidean distance mapping for computing microstructural gradients at
514 interfaces in composite materials, Cem. Concr. Res. 36 (6) (2006) 1091-1097.
515 [29] D.P. Bentz, E.J. Garboczi, E.S. Lagergren, Multi-scale microstructural modelling of concrete diffusivity:
516 Identification of significant variables, Cement Concrete Aggr. 20 (1) (1998) 129-139.
517 [30] H.S. Wong, N.R. Buenfeld, J. Hill, A.W. Harris, Mass transport properties of mature wasteform grouts,
518 Adv. Cem. Res. 18 (1) (2007) 1-12.
519 [31] B. Gérard, J. Marchand, Influence of cracking on the diffusion properties of cement-based materials,
520 Part 1: Influence of continuous cracks on the steady-state regime, Cem. Concr. Res. 30 (1) (2000) 37-43.

[32] E.J. Garboczi, L.M. Schwartz, D.P. Bentz, Modeling the influence of the interfacial zone on the DC electrical conductivity of mortar, Adv. Cem. Based Mater. 2 (5) (1995) 169-181.

[33] J.D. Shane, T.O. Mason, H.M. Jennings, E.J. Garboczi, D.P. Bentz, Effect of the interfacial transition zone on the conductivity of Portland cement mortars, J. Am. Ceram. Soc. 83 (5) (2000) 1137-1144.

List of table and figure captions

547 Table 1 Parameters used for calculating the hydration of clinker phases for ordinary Portland cement as a
548 function of time, from Parott & Killoh [15]

Parameter	Clinker phase			
	Alite	Belite	Aluminate	Ferrite
K_1	1.5	0.5	1.0	0.37
N_1	0.7	1.0	0.85	0.7
K_2	0.05	0.006	0.04	0.015
K_3	1.1	0.2	1.0	0.4
N_3	3.3	5.0	3.2	3.7

549

550

551 Table 2 Experimental design for sensitivity analysis

Test case	Simulation parameters				
	w_0/c	Curing period, t (d)	ITZ width, h (μm)	Aggregate D_{max} (mm) & gradation	Aggregate fraction, f_a
(a)	0.4, 0.5, 0.6	28	35	16 (Fuller)	0-0.6
(b)	0.5	3, 7, 14, 28, 56	35	16 (Fuller)	0-0.6
(c)	0.5	28	5, 10, 20, 35, 50	16 (Fuller)	0-0.6
(d)	0.5	28	35	8, 16, 32 (Fuller) 16 (EVF)	0-0.6

552

553

554 Table 3 Results from the sensitivity analysis showing the percentage change in D_{con}/D_p

	Parameter	Simulated range	Percentage change in D_{con}/D_p	
			f_a =0	f_a =0.6
1.	w_0/c ratio	0.4 to 0.6	+ 186	+ 134
2.	Curing period	3 to 56 days	- 59	- 42
3.	ITZ width	5 to 50μm	0	+ 27
4.	Aggregate volume fraction	0 to 0.6	- 153	
5.	Maximum aggregate diameter	8 to 32mm	0	- 14
6.	Aggregate gradation	EVF to Fuller	0	+ 19

555

556

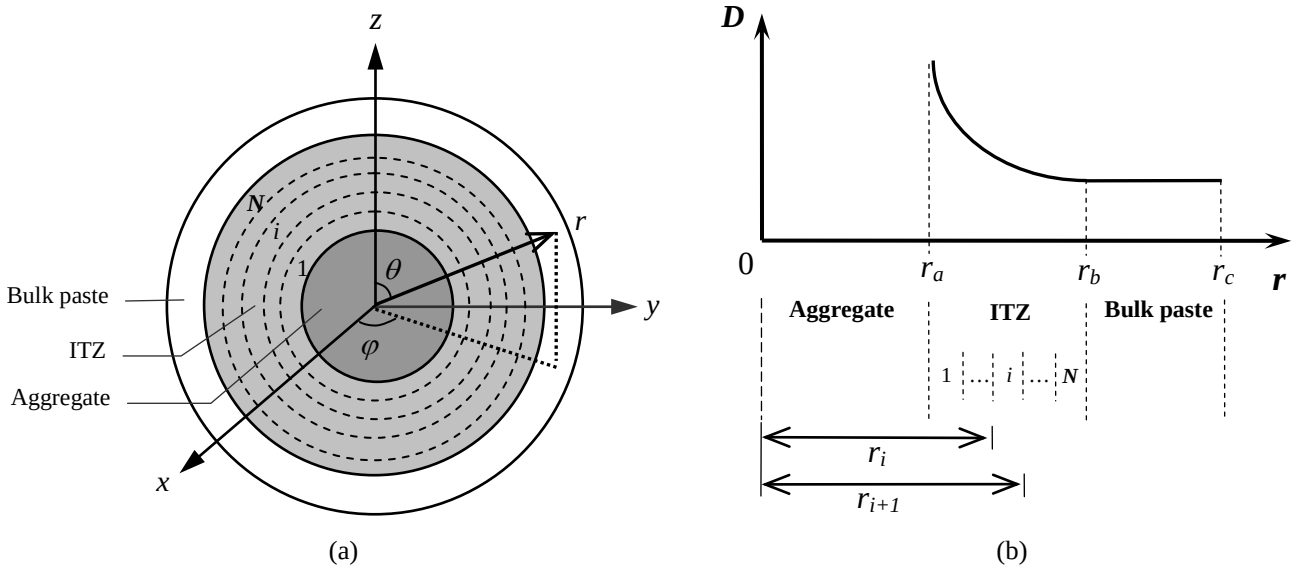

(a) (b)

557 Fig. 1 Schematics of the three-phase composite sphere model used to represent concrete. The various dimensions
558 and notations used in the model are shown.

559

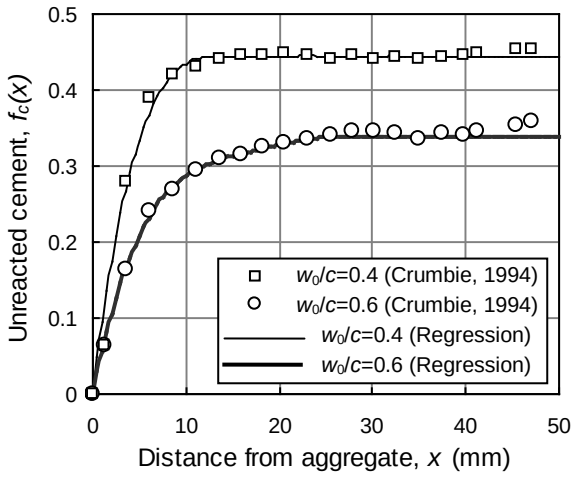

560 Fig. 2 Initial distribution of cement particles from aggregate surface at different water/cement ratios. Data is
561 obtained from experimental results of Crumbie [14], which is then fitted using Eq. (4).

562

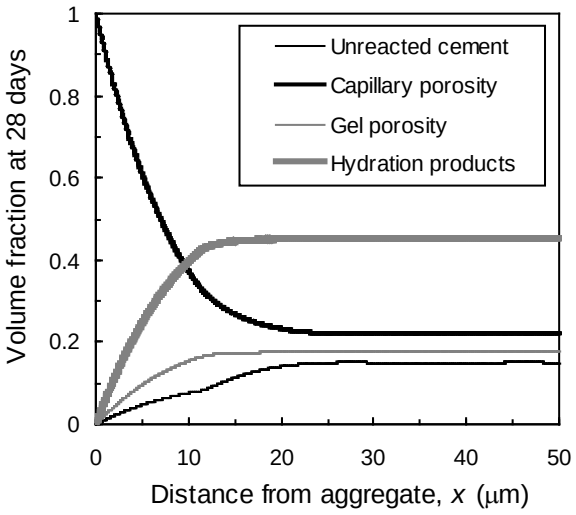

563 Fig. 3 Example of simulated gradients for a concrete hydrated for 28 days (w_0/c =0.40, ASTM Type 1 cement,

564 aggregate size: 0.15-16mm, h =25μm)

565

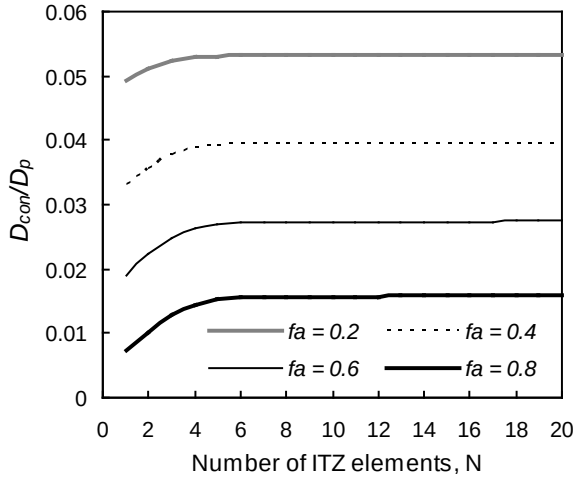

566 Fig. 4 Effect of the number of ITZ elements on the calculated diffusivity ratio D_{con}/D_p for various aggregate

567 volume fractions, f_a (w_0/c =0.50, ITZ width = 35μm, curing period = 28 days, aggregate gradation = 0.15-

568 16mm, Fuller). The simulation shows that N =10 is sufficient to obtain representative results.

569

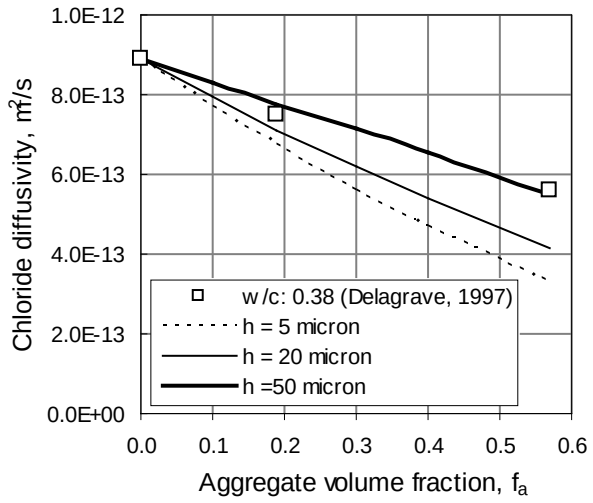

(a) Series 1 w_0/c 0.38 (from Delagrave et al [3])

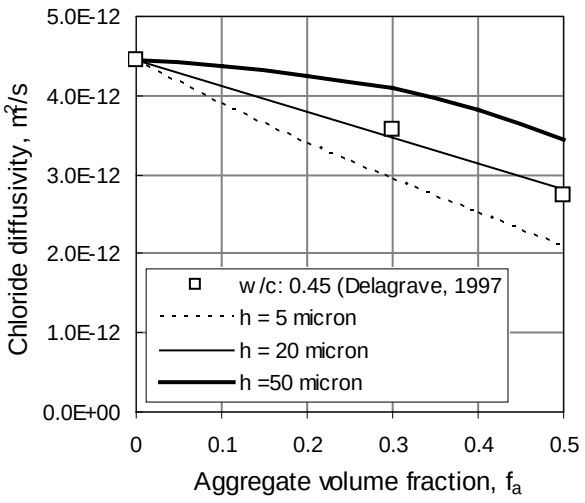

(b) Series 2 w_0/c 0.45 (from Delagrave et al [3])

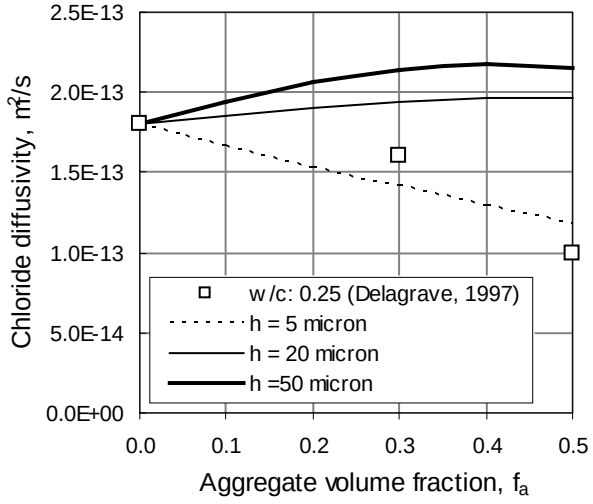

(c) Series 3 w_0/c 0.25 (from Delagrave et al [3])

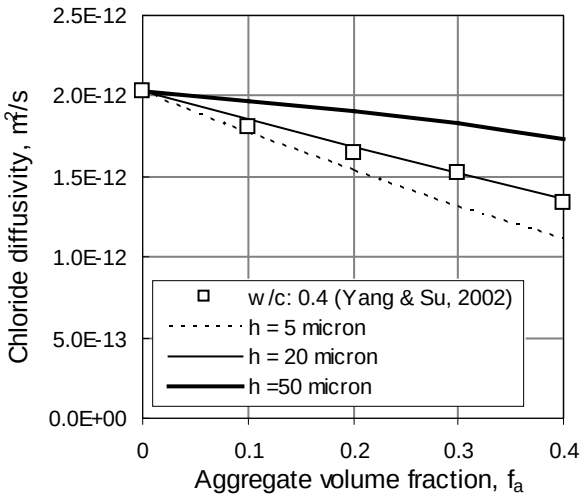

(d) w_0/c 0.4 (from Yang & Su [26])

570 Fig. 5 Comparison between the numerical simulation results with experimental results of Delagrave et al. [3] and

571 Yang & Su [26].

572

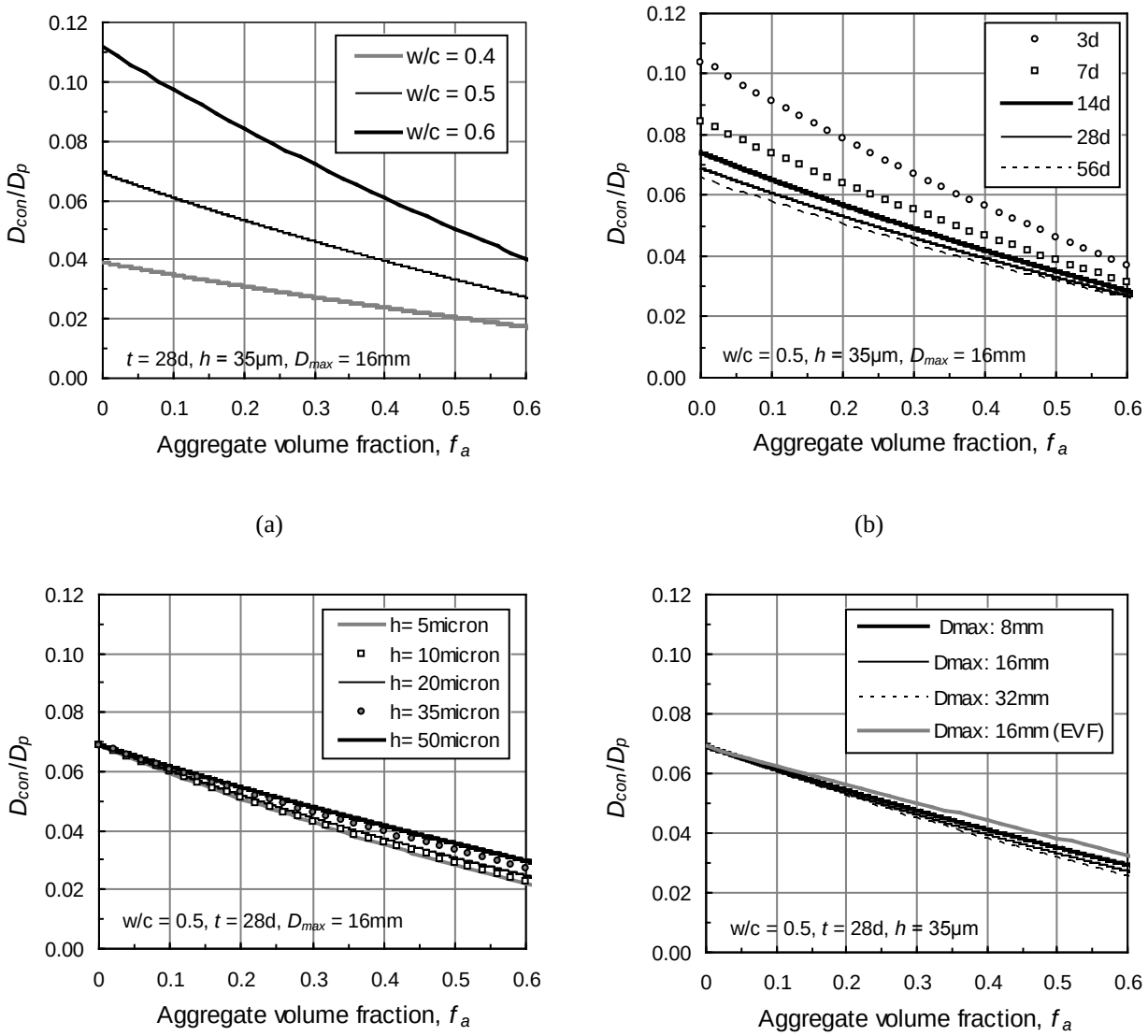

573 Fig. 6 Results from sensitivity analysis showing the effect of a) w_0/c ratio, b) curing period, c) ITZ width and d)

574 aggregate maximum size and gradation, on the simulated D_{con}/D_p

575

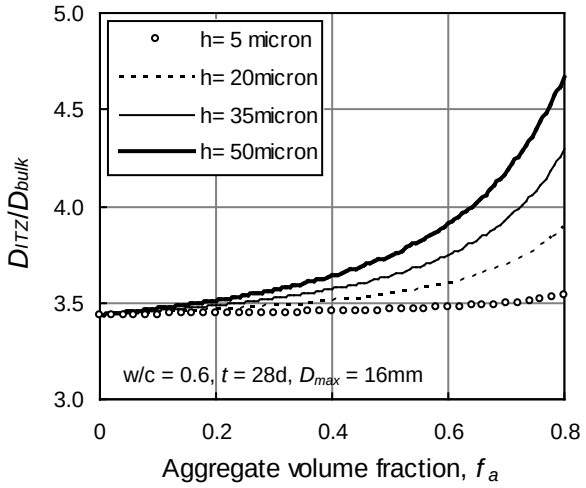

576 Fig. 7 Effect of ITZ width and aggregate content on D_{ITZ} / D_{bulk} ratio for a concrete with w_0 / c 0.6 and ASTM

577 Type 1 cement cured for 28 days.